On the impact of multi-axial stress states on trailing edge bondlines in wind turbine rotor blades

On the impact of multi-axial stress states on trailing edge bondlines in wind turbine rotor blades

Pablo Noever Castelos, Claudio Balzani
Leibniz Universität Hannover, Institute for Wind Energy Systems, Hannover, 30167, Germany
E-mail: pablo.noever@iwes.uni-hannover.de

Abstract. For a reliable design of wind turbine systems all of their components have to be designed to withstand the loads appearing in the turbine's lifetime. When performed in an integral manner this is called systems engineering, and is exceptionally important for components that have an impact on the entire wind turbine system, such as the rotor blade. Bondlines are crucial subcomponents of rotor blades, but they are not much recognized in the wind energy research community. However, a bondline failure can lead to the loss of a rotor blade, and potentially of the entire turbine, and is extraordinarily relevant to be treated with strong emphasis when designing a wind turbine.

Modern wind turbine rotor blades with lengths of 80 m and more offer a degree of flexibility that has never been seen in wind energy technology before. Large deflections result in high strains in the adhesive connections, especially at the trailing edge. The latest edition of the DNV GL guideline from end of 2015 demands a three-dimensional stress analysis of bondlines, whereas before an isolated shear stress proof was sufficient. In order to quantify the lack of safety from older certification guidelines this paper studies the influence of multi-axial stress states on the ultimate and fatigue load resistance of trailing edge adhesive bonds. For this purpose, detailed finite element simulations of the IWES IWT-7.5-164 reference wind turbine blades are performed. Different yield criteria are evaluated for the prediction of failure and lifetime.

The results show that the multi-axial stress state is governed by span-wise normal stresses. Those are evidently not captured in isolated shear stress proofs, yielding non-conservative estimates of lifetime and ultimate load resistance. This finding highlights the importance to include a three-dimensional stress state in the failure analysis of adhesive bonds in modern wind turbine rotor blades, and the necessity to perform a three-dimensional characterization of adhesive materials.

1. Introduction

Rotor blades of modern multi-megawatt wind turbines reach lengths of 80 m and more [1]. Such blades are slender and flexible structures, experiencing huge loads and large deflections. Associated with that, new challenges arise for the design and analysis of rotor blades [2]. Among others the damages of the leading edge and especially the trailing edge are common reasons for turbine blade failure [3]. Linked to that, and considering that failure of a blade may potentially lead to the loss of an entire wind turbine, the reliable design of rotor blade bondlines is crucial for designing reliable wind turbines, and thus highly relevant for wind turbine systems engineering.

This paper deals with the 3D finite-element-based failure analysis of trailing edge bondlines in large rotor blades for ultimate and fatigue loads. The simulations are based on the reference wind turbine model IWT-7.5-164 [4], which is a 7.5 MW direct drive wind turbine with 80 m long

blades, and contains a detailed lay-up of the blade structure. The design of the laminates has been done elsewhere [4]. The adhesive connections, however, were not subjected to an elaborate dimensioning process, so that assumptions are made in the next section in this concern.

The focal point of this paper is a comparison between the shear stress proof according to the 2010 edition of the Germanischer Lloyd (GL) certification guidelines [5] and a multi-axial stress proof as demanded by the latest DNV-GL guideline [6]. Wacker & Hauschildt [7] suggest a simplified engineering approach to determine the mean shear stress in the bonding according to [5], whereas for the multi-axial stress proof the analyses are based on the Tresca failure hypothesis considering a maximum shear stress and the Drucker-Prager failure hypothesis that takes into account different tensile and compressive strengths.

The simulation results support the recent modifications of the design guidelines, highlight the necessity to account for multi-axial stress states, and potentially open a discussion on the real failure mechanisms appearing in adhesive connections of wind turbine rotor blades.

2. Finite element model of the rotor blade

For the modeling of the IWT-7.5-164 reference blade a Model Creator and Analysis Tool called MoCA, which has been developed at the Institute for Wind Energy Systems at Leibniz Universität Hannover, was utilized. MoCA is MATLAB-based [8] and creates fully parameterized finite element models of wind turbine rotor blades in ANSYS [9] format using shell elements (element type number 181). An extension has been implemented for the discretization of the trailing edge bondline with solid elements (element type number 185). Two assumptions are made for the geometry of the trailing edge bondline: It has i) a width of 10 cm throughout the blade, and ii) a concave inner face shape.

Note that the aforementioned assumptions are quite rough (see also the respective comment in section 1) as the adhesive geometry normally is an outcome of a structural design. A concave shape at the inner face is generally difficult to manufacture due to restrictions in accessibility, hence convex shapes are normally realized. However, convex inner face shapes are related to high stress concentrations, whose effects on the failure mechanisms within the adhesive are not subject of this paper. As we focus on the general influence of a three-dimensional stress state, and not on advantages or disadvantages of a particular design or a particular bondline shape, the assumptions concerning the adhesive geometry seem reasonable.

The stress postprocessing is limited to a span-wise region from 41 m to 47 m for ultimate loads, and to a spanwise region from 41 m to 43 m for fatigue loads (due to computation time penalties). A mesh convergence study has been performed to guarantee reliable results. The resulting global finite element mesh and a local view on the adhesive are shown in Fig. 1.

The bondlines treated in this paper are modeled by a relatively coarse mesh of 6×18 elements in the cross section to obtain fast results and compare different approaches. Hence, the

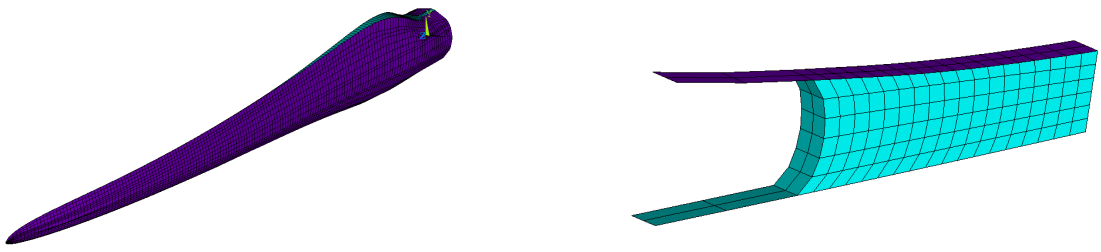

(a) (b)

Figure 1. Finite element model of the IWT-7.5-164 reference wind turbine blade: Global mesh (a) and local mesh of the adhesive (b).

Table 1. Ultimate Loads for the 80 m reference blade calculated according to [5]. The coordinate system for the applied forces is defined as in Fig. 2 (a).

Spanwise Pos. [m]	F_x [kN]	F_y [kN]	F_z [kN]	M_x [kNm]	M_y [kNm]	M_z [kNm]
29	705.6	-249.8	1176.8	5335.0	17988.1	768.4
39	606.2	-194.2	836.8	3545.7	11840.0	529.4
49	477.2	-143.8	534.8	2029.4	6791.1	375.0
59	325.4	-96.5	268.7	913.0	3002.7	203.2
69	158.6	-47.7	94.6	238.7	728.1	86.2

Table 2. Internal loads achieved through the modeling technique at spanwise positions of 41 m and 47 m (coinciding with the ends of the stress evaluation region).

Spanwise Pos. [m]	F_x [kN]	F_y [kN]	F_z [kN]	M_x [kNm]	M_y [kNm]	M_z [kNm]
41	604	-192	651	3737	11658	-527
47	604	-192	651	2586	8030	-527

postprocessing analyses disregard the outer elements in the cross section to avoid erroneous results from e.g. free edge effects or corner singularities. In this way cohesion failure is investigated and adhesion failure is neglected (since also very difficult to characterize).

All degrees of freedom at the blade root are fixed as geometric boundary conditions. Aeroelastic simulations are the basis for load-like boundary conditions, see also sections 3 and 4. When applying concentrated external loads, high geometric nonlinearities appear in both ultimate and fatigue analyses in the 3D blade model. Hence, the blade was cut at a spanwise position of 54 m and internal forces and moments from aeroelastic turbine simulations were applied as external concentrated loads at the cutted end. In this way the geometric nonlinearities could be minimized to an acceptable extent (due to the small offset of the applied loads and the evaluated elements). The loads were linearly interpolated from the aeroelastic simulation output and then distributed along the span for 1 m (between 53 m and 54 m; 4 elements are used here in span-wise direction) and across the shell of the blade via rigid MPCs (element type number 170 for the target node and element type number 177 for the contact nodes; the target node is located on the threading line). In this way displacement restrictions from the load introduction is smoothened, and the distance between the load introduction nodes and the evaluation region avoids deformation penalties in the evaluated elements.

3. Ultimate load resistance of the trailing edge bondline

The worst case scenario has been applied for the determination of the material efforts due to ultimate loads, i.e. all ultimate loads have been applied at the same time in order to have one ultimate load state shown in Tab. 1 that can easily be compared for the different failure criteria. The design load cases (DLC) from the IEC standard [11] were calculated with the aeroelastic simulation program HAWC2 [10]. From the resulting load histories the extreme values for every defined cross section in the aeroelastic system were picked, which were mainly contributed by the DLC 1.1 (Power production), DLC 2.3 (Power production with electric system fault) and DLC 6.2 (Parked). Safety factors have not been considered in the aeroelastic simulations, but in the preceding postprocessing. The resulting internal forces and moments due to the load introduction strategy described in section 2, are given in Tab. 2 at the ends of the region where the stresses are evaluated (namely at spanwise positions of 41 m and 47 m). The internal forces and the torsional moment are constant, while the bending moments are linearly distributed.

Table 3. Average adhesive strength values of experimental campaigns [12]

Property	Value
Tensile strength	41.95 MPa
Compressive strength	75.30 MPa
Shear strength	19.92 MPa

According to [5] the shear strength of the adhesive material has to be determined experimentally unless a certified adhesive is utilized. In the latter case, a simplified maximum shear stress proof can be performed using a characteristic shear strength of 7 N/mm^2, that considers a stress concentration of factor 3. For the isolated shear strength approach we utilize an engineering approximation for the mean shear stress τ_{xz} in the bondline given by

$$\tau_{xz} = \frac{Q_x \cdot S_x}{I_{yy} \cdot w_{\text{bonding}}}, \tag{1}$$

as proposed in [7]. Therein, I_{yy} is the second moment of inertia of the entire blade cross section, Q_x is the shear force in x-direction, S_x is the static moment of the bondline cross section with respect to the x-axis, which is simplified to the product of bondline cross-sectional area, A_{bonding}, and the distance of the centroid of A_{bonding} to the x-axis, Δx, i.e. $S_x = A_{\text{bonding}} \cdot \Delta x$, and w_{bonding} corresponds to the width of the trailing edge bondline. The mean shear stress τ_{yz} is calculated analogously. We neglect shear stresses τ_{xy} due to torsional loading as it leads to negligibly small values compared to τ_{xz} and τ_{yz}.

After applying a partial safety factor of $\gamma_{\text{F}} = 1.35$ for the loads and $\gamma_{\text{Md}} = 2.45$ for the material characteristics [5] the approximation according to Eq. (1) yields a maximum shear stress of $\tau_{yz,\text{max}} = 1.98$ N/mm^2 in the analyzed region. This results in a material effort of $f_{\text{max,GL}} = 0.69$, i.e. stress proof fulfilled.

In the multi-axial analysis we employ a material that has the properties listed in Tab. 3, which are average adhesive strengths of experimental campaigns [12]. The multi-axial stress state is analyzed using two failure criteria, the Drucker-Prager yield criterion [13] and the Tresca failure hypothesis [14]. The Drucker-Prager criterion was developed for materials with different tensile and compressive strengths, e.g. concrete or polymers [15]. This is also the nature of adhesives commonly used for wind turbine rotor blades (EP and PU), which show a compressive strength that is significantly higher than the tensile strength [12]. The Drucker-Prager equivalent stress is given by the expression

$$\sigma_v = \frac{m-1}{2}(\sigma_1+\sigma_2+\sigma_3) + \frac{m+1}{2}\sqrt{\frac{1}{2}[(\sigma_1-\sigma_2)^2+(\sigma_2-\sigma_3)^2+(\sigma_3-\sigma_1)^2]}, \tag{2}$$

see [15], where $m = R_t/R_c$ is the ratio between the tensile strength, R_t, and the compressive strength, R_c, and σ_1, σ_2, and σ_3 are the principal stresses, respectively, following the convention $\sigma_1 \leq \sigma_2 \leq \sigma_3$. The strength ratio m normalizes the principal stresses to the tensile strength. We calculate the maximum shear stress in the material from the three-dimensional stress state via the well-known Tresca failure hypothesis [14] which is given by the expression

$$\tau_{max} = \frac{1}{2}\max(|\sigma_1-\sigma_2|, |\sigma_2-\sigma_3|, |\sigma_3-\sigma_1|). \tag{3}$$

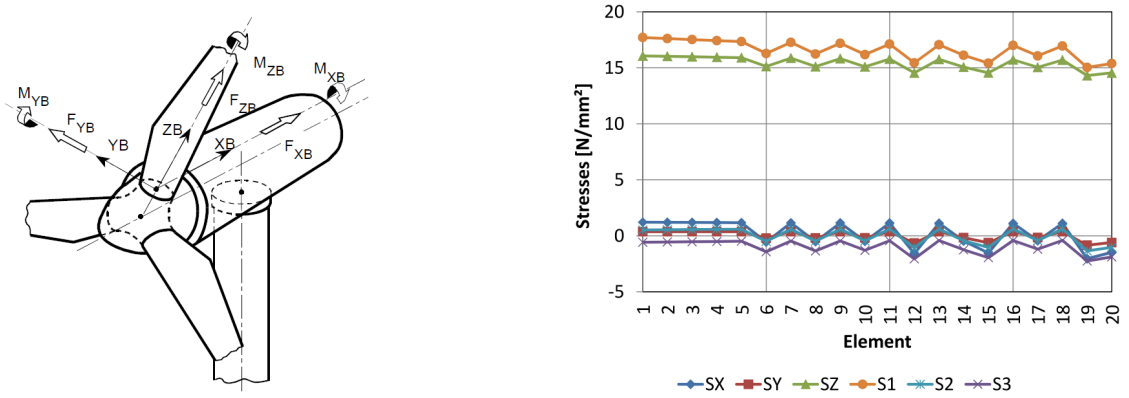

(a) (b)

Figure 2. (a) Global blade coordinate system [5]; (b) stresses in global blade coordinates and principal stresses under ultimate loads of the 20 most loaded elements.

Fig.2 (b) shows the results from the finite element analysis for the ultimate load case of the reference blade for the 20 most stressed elements in the stress evaluation region. The stresses are plotted in the global blade coordinate system (SX,SY,SZ) according to [5], which is illustrated in Fig. 2 (a), and as principal stresses (S1,S2,S3) for each element. The graph clearly shows a dominant stress in spanwise direction (z-direction), which characterizes the main principal stress direction (S1), whereas all other stresses are a small fraction of it.

Fig. 3 presents the Drucker-Prager and Tresca equivalent stresses compared to the maximum and minimum principal stresses in the 20 most stressed elements. These are mainly clustered at the end of the analysis region at a spanwise position of $R = 47$m. Additionally, the tensile and shear design strengths ($R_{\mathrm{t,d}}$ and $R_{\mathrm{s,d}}$) are outlined. From the relationship between the equivalent and the principal stresses we see that the equivalent stresses are significantly governed by the maximum principal stress S1, which in fact is approximately the stress in spanwise direction.

Furthermore, Fig. 3 shows that the Tresca equivalent shear stress exceeds the design shear strength for all shown elements reaching material efforts of up to $f_{\mathrm{max,TR}} = 1.12$, i.e. the strength proof is not fulfilled. The same holds for the Drucker-Prager equivalent stress that reaches a

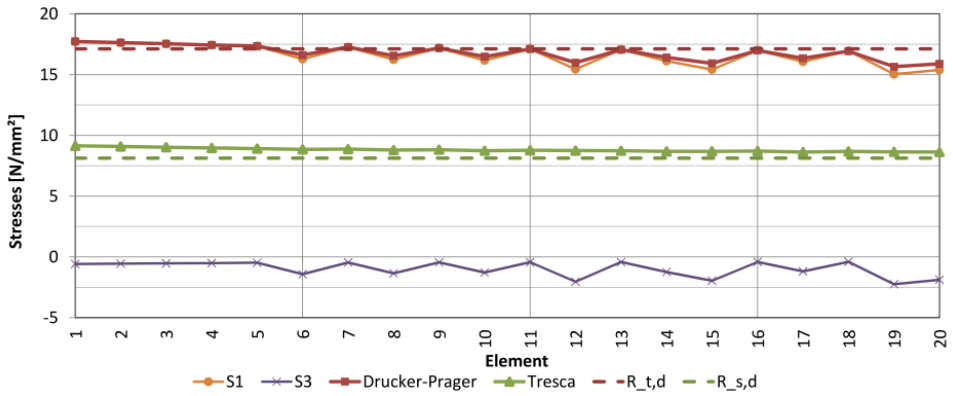

Figure 3. Equivalent stresses according to Drucker-Prager and Tresca under ultimate loads of the 20 most loaded elements and the design strength limits for tensile and shear stress.

maximum material effort of $f_{\max,\mathrm{DP}} = 1.05$. Recall that the simplified method according to [5] yields a material effort of $f_{\max,\mathrm{GL}} < 1$, i.e. no failure occurs. We can conclude that taking into account the multi-axial stress state makes the difference between no failure and failure.

The results of the ultimate load analysis for the whole analyzed region are shown in Fig. 4, comparing the Drucker-Prager and Tresca equivalent stresses to the simplified approach [7] according to the GL-Guidelines [5]. For the equivalent stresses in the cross section a stress range of the 3-fold standard deviation is illustrated. The simplified approach results in an increase of shear stress for decreasing radii, as can be expected from the shear forces shown in Tab. 1, whereas the multi-axial equivalent stresses decrease towards the root. This is due to the complex and changing relation of stiffness, multi-axial loading and position of the bondline with respect to the principal bending axis of the whole cross section. Another interesting point is the step in the stress curves of the Drucker-Prager and Tresca equivalent stresses at a spanwise position of about 45.5-46 m. We figured out that at this position the trailing edge unidirectional reinforcement has a significant amount of ply drops, hence the structural stiffness decreases significantly, especially at the trailing edge, so that stresses are redistributed to the adjacent structures including the bondline. Consequently, the strains and stresses in the bondline produced by bending moments and normal forces can be reduced substantially by trailing edge reinforcements.

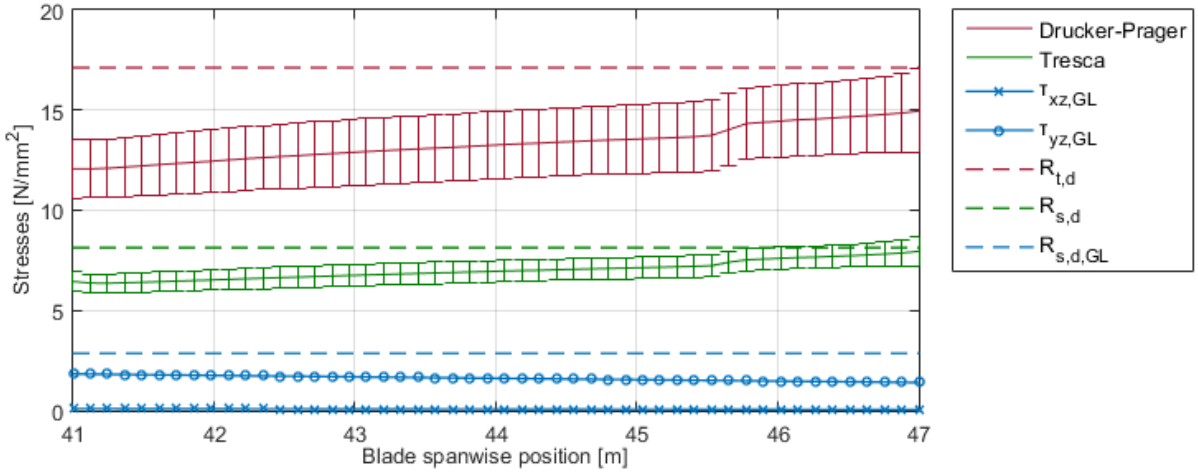

Figure 4. Spanwise view of Drucker-Prager and Tresca equivalent stresses as well as the stresses according to the simplified approach [7] demanded by the GL-Guideline [5].

4. Fatigue load resistance of the trailing edge bondline

Fatigue analyses of wind turbine components become more and more a key design issue. The degradation of the implemented materials limit the lifetime of the wind turbine or a wind turbine's component. The designing engineer has to guarantee a lifetime of at least 20 years demanded by the investment stakeholders and certification bodies. Thus the correct prediction of the components' lifetimes is of utmost importance.

Similar to ultimate load resistance analyses, the incorporation of multi-axial stress states in a fatigue analysis was not required according to [5], but an isolated shear strength analysis was sufficient. Two ways existed to fulfill those certification requirements: i) experimental material characterization with subsequent fatigue analysis on the basis of a Goodman diagram, or ii) application of the simplified approach together with a GL-certified adhesive and calculation of the damage equivalent load amplitude for 10^7 cylces, which is not allowed to exceed the limit of

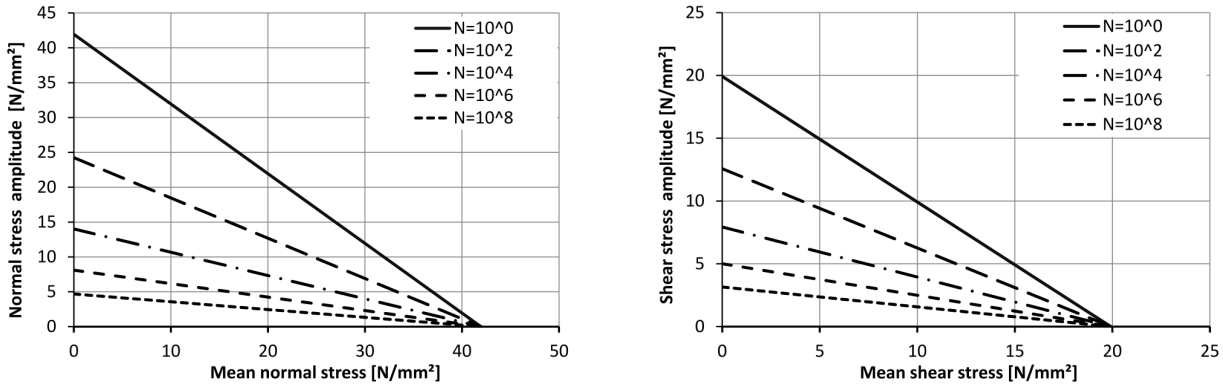

(a) (b)

Figure 5. Linear Goodman Diagram for normal stress (a) and shear stress (b).

1 N/mm^2. A multi-axial stress state as demanded from the latest DNV-GL-standard [6] has to be represented by one equivalent stress for lifetime predictions. In analogy to the first approach in [5] the calculated two-stage equivalent stress collective is evaluated using the Goodman diagram to perform the linear damage accumulation according to Palmgren & Miner [16] given by

$$D = \sum_i \frac{n_i}{N_i} \,. \tag{4}$$

Herein, n_i is the number of cycles observed for the stress state i, and N_i is the number of cycles for the stress state i that leads to fatigue failure. We use the same equivalent stress approaches for the fatigue analysis with a multi-axial stress state as in the ultimate load analysis presented in section 3, namely the Drucker-Prager and Tresca failure hypotheses. The fatigue analysis is performed for a spanwise region between 41 and 43 m in order to reduce the computational effort, see section 2.

For both the simplified and the multi-axial stress proof, the accumulated damage D has to be calculated based on Eq. (4). Therefore a load history is calculated with the aeroelastic simulation program HAWC2 [10] considering only the fatigue DLC 1.1 (Power production) according to the IEC standard [11] and a Rayleigh wind distribution with a mean wind speed of 8 m/s. The load history is evaluated using the rainflow counting method to determine the number of cycles n_i, the mean stresses $\sigma_{m,i}$, and the stress amplitudes $\sigma_{a,i}$ [17]. Furthermore, the number of cycles to failure N_i is computed by means of a Goodman-Diagram of the adhesive for normal and shear stress application (interpolated from Fraunhofer IWES internal material experiments, [12] and [18]) shown in Fig. 5. As stated before, the transformation of the multi-axial stress state to the Drucker-Prager equivalent stress normalizes the multi-axial stresses to the smallest strength value, the tensile strength. Hence, only the tensile mean stress of the Goodman-Diagram is necessary to evaluate the load history.

The evaluation of the shear stress history of the simplified approach according to [7] in Eq. (1) results in a total damage D. With that damage and a given number of cycles n_{DEL}, Eq. (4) yields the maximum number of cycles to failure, N_{DEL}. The damage equivalent load amplitude (DEL) is calculated with the so-called Wöhler curve defined by

$$\sigma_a = \sigma_{a0} \cdot N^{-\frac{1}{m}} \tag{5}$$

for alternating stresses with a mean stress $\sigma_m = 0$ [16]. In Eq. (5), σ_a is the stress amplitude, σ_{a0}

is the maximum stress amplitude for a single cycle, and m is the Wöhler exponent. According to the GL certification guidelines, the shear stress proof is satisfied if the damage equivalent load amplitude does not exceed 1 N/mm^2 for $n_{\mathrm{DEL}} = 10^7$. The calculated maximum annual total damage of the simplified shear stress approach is $D_{\tau_{\mathrm{yz}}} = 0.394$, which results in a lifetime of about 2.5 years and a damage equivalent load amplitude of $\tau_{a,yz} = 3.62$ N/mm^2 > 1 N/mm^2 ($m = 10$, $\sigma_{a0} = 19.92$ N/mm^2). Hence, the proof is not satisfied and a lifetime of 2.5 years is far below the demanded minimum of 20 years. Note that this means that the trailing edge bondline would have to be re-designed in order to fulfill the design requirements. This step is omitted in this work since the focus is the comparison of different analysis methods, and not the particular design of an adhesive connection.

For the multi-axial stress proof according to [6] this paper suggests the approaches with the Drucker-Prager and Tresca equivalent stresses for an initial fatigue analysis. Fig. 6 exemplarily shows the predicted lifetimes computed by the fatigue analysis for the Drucker-Prager equivalent stress, Fig. 6 (a), and the Tresca equivalent shear stress, Fig. 6 (b), of a cross section of the bondline at a spanwise position of $R = 41$m. Similar to the local view in Fig. 1 (b) the suction side of the blade is at the top, the pressure side is at the bottom, and the trailing edge is on the right-hand side of the figures. The results for the Drucker-Prager approach show high fatigue damages directly at the trailing edge resulting in a very low predicted lifetime with a maximum of less than three months. The analysis based on the Tresca equivalent shear stress shows similar results. The predicted lifetime in this case is about 8 months.

The predicted mean lifetime in a bondline cross section is plotted for a spanwise region between 41 m and 43 m in Fig. 7. Therein, we observe that the larger the radius, the lower the lifetime becomes. This effect is due to the complex relations between stiffness, multi-axial loading and position of the bondline with respect to the principal bending axis and was already found in the ultimate load analysis. Both multi-axial approaches show lifetime predictions of less than 3 months. The results show a higher fatigue damage considering the multi-axial stress state compared to the simplified approach. The estimated lifetime is only a fraction of the 2.5 years computed with the simplified approach of the GL certification guideline.

It should be mentioned that normal stresses in spanwise direction based on the high edgewise bending moments dominate the multi-axial stress states in fatigue as well as for the static analysis

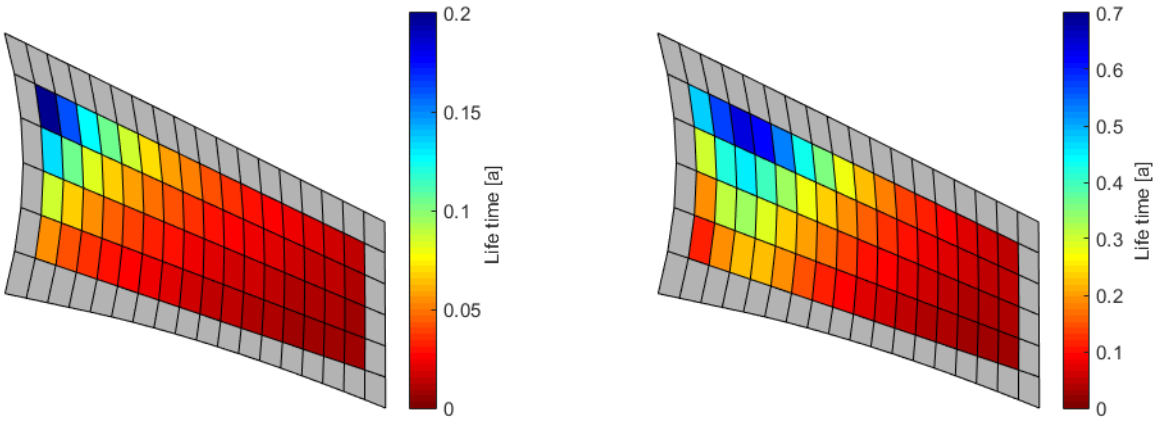

(a) (b)

Figure 6. Lifetime prediction with the Drucker-Prager equivalent stress (a) and the Tresca equivalent shear stress (b) for a bondline cross section at $R = 41$m.

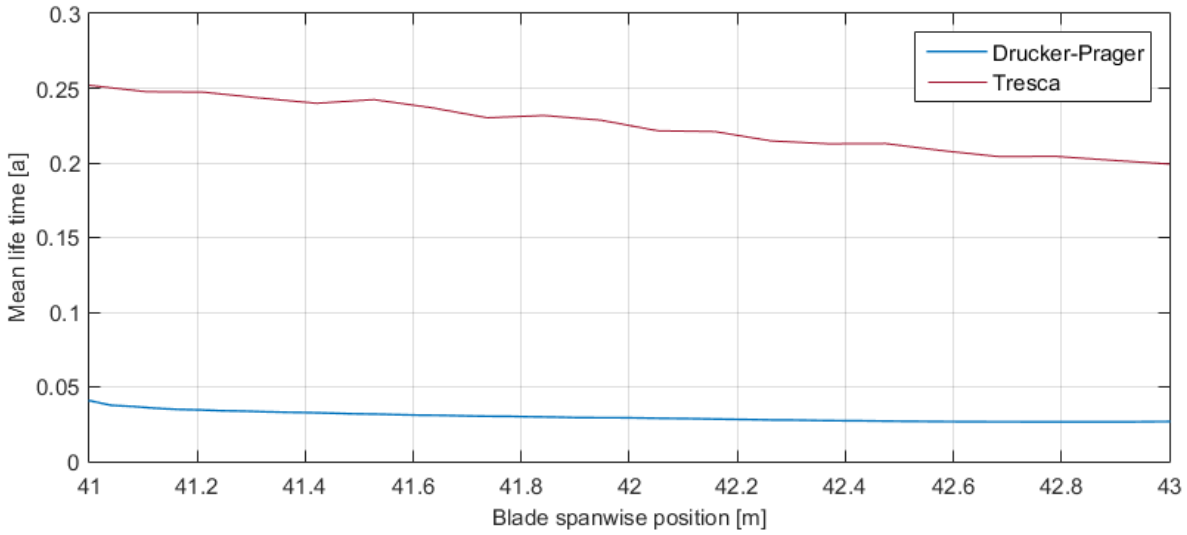

Figure 7. Cross sectional mean lifetime prediction of the bondline in the spanwise region of $R = 41 - 43$m

of ultimate load resistance, determining the direction of one of the principal axes. Due to non-proportional loading the directions of the remaining two principal axes change throughout the load history. This makes an interpretation of the results difficult, as both multi-axial approaches do not consider the direction of the critical plane in every step in the load history. Thus, the accumulation of all damages without considering the plane of action yields an underestimation of the lifetime predictions, which has to be considered in future investigations.

5. Conclusions

According to the latest version of the GL guidelines for wind turbine rotor blade design, a stress proof for bondlines is required that takes into account a 3D stress state, instead of limiting to an isolated shear stress proof as was demanded by older GL guidelines. However, there is no method established for an accurate consideration of a three-dimensional stress state. Hence, this paper studied two different three-dimensional failure hypotheses, namely the Drucker-Prager and the Tresca failure criteria, and compared the respective finite element based predictions with a simplified shear stress proof according to older GL guidelines. Those comparisons have been performed for both ultimate and fatigue strength analysis of a trailing edge bondline.

It was shown that incorporating a multi-axial stress state in the failure analysis of a trailing edge bondline results in significantly larger material efforts in the adhesive compared to an isolated shear strength analysis. This holds for both quasi-static ultimate strength and fatigue analysis. In the case of a fatigue assessment the high material efforts are linked to remarkably shorter lifetimes (if a traditional fatigue analysis concept is followed, where the first macroscopic damage is interpreted as end of life). Shorter lifetimes have been estimated utilizing both the Drucker-Prager and the Tresca failure criteria, supporting the recent modifications of the GL guidelines. An evaluation of more advanced methods such as the critical plane fatigue approach [19] or fracture mechanical approaches could be useful in estimating numerically the impact of a 3D stress state on the failure mechanisms of bondlines in wind turbine rotor blades.

It was also shown that the higher efforts in the trailing edge adhesive are a consequence of high longitudinal normal stresses due to blade bending, which most probably result in transverse cracks within the adhesive (since a crack normally formates perpendicular to the

major stress component). Transverse cracks not necessarily correspond to final failure of the blade, since stress redistributions from the adhesive to the adherents could increase the load-carrying capacity of the blade, offering the opportunity to further exploit material reserves. In this case nonlinearities would be introduced in the fatigue stress-strength relations that cannot be captured in today's fatigue analyses, which then requires novel design concepts. On the other hand, stress concentrations in the vicinity of the transverse cracks may as well affect the structural integrity of both adhesive and adherents, leading to final failure of the blade when the first transverse crack in the adhesive appears, and thus to shorter lifetimes. Consequently, in the latter case blades designed according to the former GL guidelines run the risk of not surviving the approved lifetime and the respective turbines may be prone to entire blade replacements (or severe retrofitting actions).

The authors would like to emphasize that the numerical findings of this paper have to be verified by experimental investigations. Especially the strength hypotheses utilized in this work have to be thoroughly characterized by experiments. Further, there is a strong lack of knowledge concerning the real failure mechanisms appearing in the adhesive and the adherents, at least in literature. The scenarios described in the last paragraph are strictly contrary and are just two out of an almost infinite number of possibilities. From this it is clear that fundamental research, both in an experimental and a numerical framework (or ideally in a joint fashion), is absolutely necessary to clarify the real failure mechanisms of bondlines in wind turbine rotor blades, and to capture them in simulation environments for design processes.

References

[1] Katnam K B, Comer A J, Roy D, da Silva, L F M and Young T M 2014 *The Journal of Adhesion* **91** 113–139 ISSN 0021-8464
[2] Hayman B, Wedel-Heinen J and Brøndsted P 2008 *MRS Bulletin* **33**
[3] Sørensen B, Toftegaard H, McGugan M, Pereira G and Branner K 2015 Very large wind turbine rotor blades require damage tolerance and damage monitoring
[4] Sevinc A, Rosemeier M, Bätge M, Braun R, Meng F, Shan M, Horte D, Balzani C and Reuter A 2016 *Reference Wind Turbine IWT-7.5-164 Specification*
[5] Germanischer Lloyd Industrial Services GmbH 2010 *Richtlinie für die Zertifizierung von Windenergieanlagen* (Hamburg: Germanischer Lloyd)
[6] DNV GL AS 2015 *DNVGL-ST-0376 - Rotor blades for wind turbines*
[7] Wacker G and Hauschildt M 2003 *Klebverbindungen in Rotorblättern für Windenergieanlagen* (Hamburg)
[8] The MathWorks I 2016 *MATLAB Primer*
[9] ANSYS Inc 2013 *ANSYS Mechanical APDL Theory Reference*
[10] Larsen T J and Hansen A M 2015 *How 2 HAWC2, the user's manual* (*Risø R, Report* vol 1597) (Roskilde: Risø National Laboratory)
[11] IEC 61400-1 2007 *International Standard: Wind turbines - Part 1: Design requirements* 3rd ed (*International standard Norme internationale* vol CEI 61400-1) (Geneva: International Electrotechnical Commission) ISBN 2831881617
[12] Zarouchas D and van Hemelrijck D 2012 *Journal of Adhesion Science and Technology* **28** 1500–1516 ISSN 0169-4243
[13] Alejano L R and Bobet A 2012 *Rock Mechanics and Rock Engineering* **45** 995–999 ISSN 0723-2632
[14] Issler L, Ruoß H and Häfele P 2006 *Festigkeitslehre - Grundlagen* 2nd ed Springer-Lehrbuch (Berlin: Springer) ISBN 10 3-540-40705-7
[15] Stark R 2006 *Festigkeitslehre: Aufgaben und Lösungen* (Vienna: Springer-Verlag/Wien) ISBN 10 3-211-29699-9
[16] Freebury G and Musial W 2000 *Determining equivalent damage loading for full-scale wind turbine blade fatigue tests*
[17] Köhler M, Jenne S, Pötter K and Zenner H 2012 *Zählverfahren und Lastannahme in der Betriebsfestigkeit* (Dordrecht: Springer) ISBN 978-3-642-13163-9
[18] 3M Renewable Energy Division *3M Wind Blade Bonding: Technical Data* (St. Paul)
[19] Karolczuk A and Macha E 2005 *International Journal of Fracture* **134** 267–304 ISSN 0376-9429